

## Correlation between excitation index and Eddington ratio in radio galaxies

Jing-Fu Hu<sup>1,4</sup>, Xin-Wu Cao<sup>2,3</sup>, Liang Chen<sup>1</sup> and Bei You<sup>5</sup>

<sup>1</sup> Key Laboratory for Research in Galaxies and Cosmology, Shanghai Astronomical Observatory, Chinese Academy of Sciences, Shanghai 200030, China; *hujingfu@shao.ac.cn, chenliang@shao.ac.cn*

<sup>2</sup> Shanghai Astronomical Observatory, Chinese Academy of Sciences, Shanghai 200030, China; *cxw@shao.ac.cn*

<sup>3</sup> Key Laboratory of Radio Astronomy, Chinese Academy of Sciences, 210008 Nanjing, China

<sup>4</sup> University of Chinese Academy of Sciences, Beijing 100049, China

<sup>5</sup> Nicolaus Copernicus Astronomical Center, Polish Academy of Sciences, Bartycka 18, 00-716, Warsaw, Poland

Received 2015 September 22; accepted 2016 May 4

**Abstract** We use a sample of 111 radio galaxies with redshift  $z < 0.3$  to investigate their nuclear properties. The black hole masses of the sources in this sample are estimated with the velocity dispersion/luminosity of the galaxies, or the width of the broad-lines. We find that the excitation index, the relative intensity of low and high excitation lines, is correlated with the Eddington ratio for this sample. The size of the narrow-line region (NLR) was found to vary with ionizing luminosity as  $R_{\text{NLR}} \propto L_{\text{ion}}^{0.25}$  (Liu et al. 2013). Using this empirical relation, we find that the correlation between the excitation index and the Eddington ratio can be reproduced by photoionization models. We adopt two sets of spectral energy distributions (SEDs), with or without a big blue bump in ultraviolet as the ionizing continuum, and infer that the modeled correlation between the excitation index and the Eddington ratio is insensitive to the applied SED. This means that the difference between high excitation galaxies and low excitation galaxies is not caused by the different accretion modes in these sources. Instead, it may be caused by the size of the NLR.

**Key words:** accretion, accretion disks — black hole physics — galaxies: active

### 1 INTRODUCTION

Radio galaxies are classified as Fanaroff-Riley (FR) I or FR II sources according to their radio morphology (Fanaroff & Riley 1974). FR I radio galaxies have an edge-darkened radio structure, while FR II galaxies are defined by edge-brightened radio jets terminating in compact hot spots. The jet power of FR I radio galaxies is systematically higher than that of FR IIs. The transition luminosity for FR I/II at  $P_{178\text{MHz}} \approx 10^{25} \text{ W Hz}^{-1} \text{ sr}^{-1}$ . The reason for such difference between FR I and FR II galaxies is still unclear. There are different interpretations for the FR dichotomy, such as the interaction of the jet with the ambient medium or the intrinsic nuclear properties of accretion and jet formation processes (e.g. Gopal-Krishna & Wiita 1988; Baum et al. 1995; Bicknell 1995; Reynolds et al. 1996; Blundell & Rawlings 2000; Cao & Rawlings 2004).

The central structures and activities of radio galaxies are important for understanding the physics of their nuclei. Many works have been carried out to explore the origin of the FR I/FR II division. Ledlow & Owen (1996) showed that the division between FR I and FR II radio galaxies is a function of the host galaxy's optical luminosity and the total radio luminosity. The dividing line between FR I/FR II is a linear function of the optical lumi-

osity of the host galaxy. Almost all FR II radio sources are in the region above the dividing line in the galaxy optical luminosity–radio luminosity plane, but FR Is are mostly below the dividing line. Ghisellini & Celotti (2001) converted the optical magnitude of the host galaxy to the mass of its central black hole, and derived the jet power from the radio luminosity. They showed that the dividing line between FR I and FR II radio sources in fact corresponds to a constant Eddington ratio for jet power. This implies that the FR I/FR II division may be caused by different accretion modes. FR II galaxies may contain standard thin accretion disks (Shakura & Sunyaev 1973), while advection dominated accretion flows (ADAFs) may be in FR Is (Narayan & Yi 1994).

In the unified scheme for active galactic nuclei (AGNs), orientation has a major influence on the appearance of AGNs. FR II radio galaxies and radio-loud quasars are intrinsically the same but viewed from different angles (see Urry & Padovani 1995 for a review). This can also apply to FR I radio galaxies and BL Lac objects. A similar dividing line between radio quasars and BL Lac objects has also been found by Xu et al. (2009).

Cao & Rawlings (2004) analyzed the optical and radio properties of a sample of 3CR FR I radio galaxies and argued that a few FR Is in their sample may contain standard

thin disks. If ADAFs or adiabatic inflow-outflow solution (ADIOS) flows are present in these sources, the Blandford-Znajek mechanism is unable to generate the high power jets in these sources (Blandford & Znajek 1977). Wold et al. (2007) studied the effect of nuclear activities on the FR I/FR II division in a sub-sample of 3CR radio galaxies ( $z < 0.2$ ). They concluded that the FR I/FR II division is dominated by the central activities of nuclei, but the external environment also has influence on the dichotomy. Indeed, there are some hybrid sources having double structures with both an FR I jet and FR II lobes (Gopal-Krishna & Wiita 2000).

Besides the FR I/II dichotomy, radio galaxies can also be classified by their spectroscopic nuclear properties. Laing et al. (1994) carried out an optical classification on a sub-sample of 3CR radio galaxies. They proposed that FR II radio galaxies can be separated into high excitation galaxies (HEGs) and low excitation galaxies (LEGs): HEGs have  $[\text{O III}]/\text{H}\alpha > 0.2$  and equivalent width of  $[\text{O III}] > 3 \text{ \AA}$ , while LEGs have relatively weaker  $[\text{O III}]$ . Buttiglione et al. (2010) performed an optical spectroscopic survey of the 3CR sample of radio galaxies and suggested an excitation index (EI) as a new spectroscopic indicator. The EI is defined as  $\log [\text{O III}]/\text{H}\beta - 1/3 (\log [\text{N II}]/\text{H}\alpha + \log [\text{S II}]/\text{H}\alpha + \log [\text{O I}]/\text{H}\alpha)$ , representing the relative intensity of low and high excitation emission lines. They found that the 3CR radio galaxies have a bimodal distribution of EI and suggested that radio galaxies can be classified into two sub-populations according to their spectroscopic properties, i.e., the threshold of  $\text{EI} \sim 0.95$ . They speculated that the distinction may be caused by different accretion modes in these two kinds of the sources, i.e., hot gas is accreted in LEGs, while HEGs are powered by cold accreting material. They also showed that LEGs and HEGs are well separated by the line  $L_{\text{ion}}/L_{\text{Edd}} = 0.001$ , but only coexist over the range  $4 \times 10^{-4} \lesssim L_{\text{ion}}/L_{\text{Edd}} \lesssim 2 \times 10^{-3}$ . Although HEGs have systematically higher nuclear luminosities than LEGs, a few LEGs are bright radio sources and have typical FR II morphology distinguishable from HEGs.

In this work, we examine the relationship between EI and the Eddington ratio for a sample of radio galaxies. Section 2 presents the selection of the sample, while in Section 3 we show the relationship between EI and Eddington ratio. In Section 4 we describe our photoionization model and show the model results. In Section 5 we discuss the consequences of our results and summarize our conclusions. The cosmological parameters  $H_0 = 71 \text{ km s}^{-1} \text{ Mpc}^{-1}$ ,  $\Omega_\Lambda = 0.73$  and  $\Omega_m = 0.27$  have been adopted in this work.

## 2 SAMPLE AND DATA

In this work, we intend to investigate the relation between nuclear properties and EI. The EI can be calculated with

emission line fluxes,

$$\text{EI} = \log \frac{[\text{O III}]}{\text{H}\beta} - \frac{1}{3} \left( \log \frac{[\text{N II}]}{\text{H}\alpha} + \log \frac{[\text{S II}]}{\text{H}\alpha} + \log \frac{[\text{O I}]}{\text{H}\alpha} \right). \quad (1)$$

EI represents the overall ratio of high to low excitation emission lines in each source and is more stable than single line ratios (Buttiglione et al. 2010).

We selected 83 radio galaxies listed in Buttiglione et al. (2009) by applying a limited redshift range of  $z < 0.3$ , in which all the bright lines, i.e.,  $\text{H}\beta$ ,  $[\text{O III}]$ ,  $[\text{O I}] \lambda 6300$ ,  $\text{H}\alpha$ ,  $[\text{N II}] \lambda 6583$  and  $[\text{S II}] \lambda 6716/6731$  are measured.

They compiled a sample of 113 3CR radio sources with  $z < 0.3$  which include a significant number of powerful classical FR IIs, as well as FR Is, but only 83 sources have detections of all the emission lines, so we collect these 83 sources in our sample. In addition, broad  $\text{H}\alpha$  lines are seen in 15 galaxies from the selected 83 sources.

Then Son et al. (2012) (hereafter S2012) compiled a sample of 34 young radio galaxies (YRGs) as the lifetime of large radio sources is much longer than the transition timescale of the physical states in the accretion disk (O’Dea et al. 2009; Wu 2009). So, we also include 28 YRGs which all have detections of the same emission lines in the literature. The final sample analyzed in this work consists of 111 radio galaxies (56 FR IIs, 27 FR Is and 28 YRGs), in which 24 galaxies have a broad-line component and the other 87 sources do not have broad emission lines.

As done in S2012, the black hole masses of eight YRGs with broad emission lines are estimated using the single-epoch mass estimate method (McGill et al. 2008), based on the assumption that the clouds in the broad-line region are virialized (e.g., Kaspi et al. 2000; Woo & Urry 2002; McGill et al. 2008; Shen et al. 2008). For the other 20 YRGs without broad emission lines, the black hole masses are estimated from the stellar velocity dispersion of the host galaxy using the  $M_{\text{BH}} - \sigma_*$  relation (Gültekin et al. 2009). The  $\sigma_*$  measurements for 83 3CR radio galaxies are unavailable, but their black hole masses are estimated from the  $H$ -band luminosity of their host galaxies using the  $M_{\text{BH}} - L_{\text{H}}$  relation (Marconi & Hunt 2003).

We estimate the ionizing luminosity from the  $[\text{O III}]$  luminosity using the  $L_{\text{ion}} - L_{[\text{O III}]}$  relation (Buttiglione et al. 2010), as this emission line is a good indicator of the ionizing luminosity (e.g., Ghisellini & Celotti 2001). Thus the Eddington ratios of the sources in our sample are derived, which are listed in Table 1 (the Eddington luminosity is defined as  $L_{\text{Edd}} = 1.3 \times 10^{38} M_{\text{BH}}/M_\odot \text{ erg s}^{-1}$ ). The data on the emission lines are summarized in Table 1.

## 3 STATISTICAL RESULTS

We plot the EI versus the Eddington ratio  $\lambda_{\text{Edd}}$  in Figure 1. The Eddington ratio  $\lambda_{\text{Edd}}$  of our sample covers a wide range ( $\sim 10^{-6}$  to  $\sim 10^{-1}$ ), and the EIs are in the range

**Table 1** Sample Properties

Name	$z$	AGN type		$\log M_{\text{BH}}$	$\log L_{\text{Edd}}$	Name	$z$	AGN type		$\log M_{\text{BH}}$	$\log L_{\text{Edd}}$
(1)	(2)	(3)	(4)	( $M_{\odot}$ )	( $\text{erg s}^{-1}$ )	(1)	(2)	(3)	(4)	( $M_{\odot}$ )	( $\text{erg s}^{-1}$ )
				(5)	(6)					(5)	(6)
3C 15	0.073	I	2	9	47.1	3C 317	0.034	I	2	9.3	47.4
3C 17	0.22	II	1	8.7	46.8	3C 321	0.097	II	2	9.1	47.2
3C 18	0.188	II	1			3C 323.1	0.264	II	1	9.6	47.7
3C 20	0.175	II	2	8.7	46.8	3C 327	0.104	II	2		
3C 28	0.195	I	2			3C 332	0.151	II	1	9	47.1
3C 29	0.045	I	2	9	47.1	3C 338	0.032	I	2	9.4	47.5
3C 31	0.017	I	2	9.1	47.2	3C 349	0.206	II	2	8.7	46.8
3C 33	0.06	II	2	8.7	46.8	3C 353	0.03	II	2	8.7	46.8
3C 33.1	0.181	II	1	8.6	46.7	3C 371	0.05	I	2	9	47.1
3C 40	0.019	I	2			3C 379.1	0.256	II	2	9.2	47.3
3C 61.1	0.184	II	2	8.1	46.2	3C 382	0.058	II	1	9.3	47.4
3C 63	0.173	I	2			3C 386	0.017	I	2	8.6	46.7
3C 66B	0.022	I	2	9.4	47.5	3C 388	0.091	II	2	9.4	47.5
3C 79	0.256	II	2	9	47.1	3C 390.3	0.056	II	1	8.8	46.9
3C 84	0.018	I	2	9.3	47.4	3C 401	0.201	II	2	8.8	46.9
3C 88	0.03	II	2	8.7	46.8	3C 403	0.059	II	2	9	47.1
3C 93.1	0.243	I	2			3C 403.1	0.056	I	2	8.5	46.6
3C 98	0.03	II	2	8.5	46.6	3C 410	0.249	II	1		
3C 105	0.089	II	2	8.5	46.6	3C 424	0.127	I	2	8.3	46.4
3C 123	0.218	I	2	9.6	47.7	3C 433	0.102	I	2	9.2	47.3
3C 133	0.278	II	2	9	47.1	3C 442	0.026	I	2		
3C 135	0.125	II	2	8.6	46.7	3C 449	0.017	I	2	8.7	46.8
3C 136.1	0.064	II	2	8.9	47	3C 452	0.081	II	2	8.8	46.9
3C 153	0.277	II	2	9.1	47.2	3C 456	0.233	II	2		
3C 165	0.296	II	2	9.2	47.3	3C 458	0.289	II	2		
3C 166	0.245	II	2	9	47.1	3C 459	0.22	II	2	9	47.1
3C 171	0.238	II	2	8.7	46.8	3C 460	0.269	II	2		
3C 180	0.22	II	2	8.8	46.9	3C 465	0.03	I	2	9.5	47.6
3C 184.1	0.118	II	1	8.5	46.6	0025+006	0.104	CSS	2	7.2	45.3
3C 192	0.06	II	2	8.7	46.8	0134+329	0.367	CSS	1	8.6	46.7
3C 196.1	0.198	II	2	9	47.1	0221+276	0.31	CSS	1	8.7	46.8
3C 197.1	0.128	II	1	8.8	46.9	0316+413	0.018	CSO	1	7	45.1
3C 213.1	0.194	II	2	8.8	46.9	0345+337	0.243	CSS	2	8.6	46.7
3C 219	0.175	II	1	9.2	47.3	0428+205	0.219	GPS	2	8.7	46.8
3C 223	0.137	II	2	8.7	46.8	0605+480	0.277	CSS	2	9.2	47.3
3C 223.1	0.107	II	2	8.8	46.9	0754+401	0.066	CSS	2	7.4	45.5
3C 227	0.086	II	1	8.8	46.9	0810+077	0.112	CSS	2	8.5	46.6
3C 234	0.185	II	1	9.3	47.4	0921+143	0.136	CSS	2	8.6	46.7
3C 236	0.099	II	2	9	47.1	0931+033	0.225	CSS	2	9.1	47.2
3C 264	0.022	I	2	8.9	47	0941-080	0.228	GPS	2	7.7	45.8
3C 270	0.007	I	2	8.8	46.9	1007+142	0.213	CSS	2	9.1	47.2
3C 272.1	0.004	I	2	8.6	46.7	1037+302	0.091	CSS	2	8.2	46.3
3C 274	0.004	I	2	9	47.1	1154+435	0.23	CSS	1	7.9	46
3C 277.3	0.086	II	2	8.8	46.9	1203+645	0.372	CSS	1	8.4	46.5
3C 285	0.079	II	2	8.6	46.7	1233+418	0.25	CSS	2	7.9	46
3C 287.1	0.216	II	1	9.2	47.3	1250+568	0.32	CSS	1	8.3	46.4
3C 288	0.245	II	2	9.3	47.4	1323+321	0.368	GPS	2	9.2	47.3
3C 293	0.045	I	2	9	47.1	1345+125	0.122	CSS	1	7.3	45.4
3C 296	0.025	I	2	9.3	47.4	1404+286	0.077	GPS	1	8.7	46.8
3C 300	0.272	II	2	8.8	46.9	1407+363	0.148	CSS	2	7.8	45.9
3C 303	0.141	II	1	9	47.1	1521+324	0.11	CSS	2	7.3	45.4
3C 303.1	0.269	II	2			1558+536	0.179	CSS	2	8.4	46.5
3C 305	0.042	II	2	9	47.1	1601+528	0.106	CSS	1	8.5	46.6
3C 310	0.054	II	2	8.8	46.9	1610+407	0.151	CSS	2	8.2	46.3
3C 314.1	0.12	I	2			1807+698	0.051	CSS	2	8.6	46.7
3C 315	0.108	I	2	8.7	46.8	2352+495	0.238	GPS	2	8.6	46.7

Columns: (1) Target name; (2) Redshift; (3) Radio AGN type I: FR I Radio Galaxies; II: FR II Radio Galaxies; (The young compact radio galaxies are classified as: CSO: compact symmetric objects with a linear scale  $\leq 1$  kpc; GPS: gigahertz-peaked spectrum ( $\leq 1$  kpc) sources; CSS: compact steep-spectrum ( $\lesssim 20$  kpc) sources (O’Dea et al. 2009)); (4) Spectroscopic AGN type – 1: Type 1 AGN with broad emission lines; 2: Type 2 AGN without broad emission line; (5) Black Hole Mass; (6) Eddington Luminosity.

0 – 2 for most of the sources. The EIs are found to correlate significantly with the Eddington ratio  $\lambda_{\text{Edd}}$ , with a Spearman correlation coefficient of  $\rho = 0.80$  and  $p = 8.37 \times 10^{-13}$ .

The ordinary least-squares (OLS) fitting to the correlation EI- $\lambda_{\text{Edd}}$  gives

$$\text{EI} = 0.374 \log \lambda_{\text{Edd}} + 2.48. \quad (2)$$

**Table 2** Emission Line Measurements

Name (1)	H $\alpha$ (2)	[N II] $\lambda$ 6584 (3)	[S II] $\lambda$ $\lambda$ 6716, 6731 (4)	[O I] $\lambda$ 6300 (5)	[O III] $\lambda$ 5007 (6)	H $\beta$ (7)	EI (8)	$L_{\text{ion}}/L_{\text{Edd}}$ (9)
3C 15	-14.70	2.06	0.73	0.29	1.58	0.32	0.814	-3.635
3C 17	-14.27	0.70	0.44	0.44	1.28	0.24	1.016	-2.022
3C 18	-14.06	1.13	0.80	0.43	4.17	0.33	1.238	
3C 20	-14.55	0.91	0.59	0.15	1.48	0.26	1.204	-2.393
3C 28	-14.52	0.92	0.55	0.17	0.28	0.53	0.078	
3C 29	-14.60	1.85	1.02	0.19	1.07	0.24	0.798	-4.215
3C 31	-13.96	0.99	0.69	0.14	0.43	0.15	0.797	-4.877
3C 33	-13.29	0.63	0.72	0.25	3.55	0.31	1.374	-1.804
3C 33.1	-14.11	0.57	0.48	0.25	2.80	0.22	1.493	-1.554
3C 40	-14.79	2.32	1.33	0.24	1.38	0.32	0.678	
3C 61.1	-13.92	0.31	0.31	0.08	2.63	0.25	1.727	-0.934
3C 63	-14.38	0.29	0.31	0.23	1.22	0.23	1.365	
3C 66B	-13.90	2.45	0.56	0.26	0.87	0.22	0.746	-4.630
3C 79	-13.91	0.32	0.23	0.05	2.97	0.29	1.822	-1.366
3C 84	-12.55	1.12	1.05	0.64	2.09	0.42	0.738	-2.960
3C 88	-14.33	2.39	1.76	0.50	1.44	0.29	0.588	-3.872
3C 93.1	-13.89	1.36	1.09	0.28	2.08	0.28	0.998	
3C 98	-13.79	0.76	0.57	0.15	3.01	0.25	1.476	-2.813
3C 105	-14.39	1.59	1.10	0.38	3.59	0.26	1.199	-2.330
3C 123	-14.18	2.34	0.83	0.25	1.09	0.61	0.357	-2.834
3C 133	-13.97	0.70	0.31	0.25	2.26	0.32	1.271	-1.507
3C 135	-14.09	0.80	0.60	0.18	3.40	0.33	1.367	-1.804
3C 136.1	-13.57	0.59	0.40	0.05	1.08	0.14	1.530	-2.739
3C 153	-14.77	1.21	0.87	0.36	1.07	0.23	0.808	-2.749
3C 165	-15.00	1.14	0.65	0.31	1.68	0.44	0.795	-2.802
3C 166	-14.75	0.73	0.75	0.38	1.40	0.42	0.750	-2.589
3C 171	-13.78	0.57	0.67	0.24	2.73	0.36	1.226	-1.085
3C 180	-14.36	0.69	0.47	0.10	3.53	0.25	1.646	-1.733
3C 184.1	-13.77	0.27	0.20	0.08	2.71	0.29	1.759	-1.508
3C 192	-13.97	0.71	0.61	0.11	2.48	0.30	1.358	-2.612
3C 196.1	-14.48	1.19	1.01	0.20	0.91	0.22	0.823	-2.798
3C 197.1	-14.93	0.76	0.60	0.33	1.69	0.37	0.934	-3.153
3C 213.1	-15.02	1.41	0.66	0.46	1.13	0.21	0.854	-3.050
3C 219	-14.38	0.90	0.48	0.44	1.67	0.25	1.065	-2.655
3C 223	-14.01	0.63	0.46	0.19	3.09	0.23	1.548	-1.810
3C 223.1	-14.30	0.81	0.41	0.06	2.63	0.28	1.540	-2.497
3C 227	-14.17	0.19	0.32	0.08	4.73	0.44	1.802	-2.304
3C 234	-13.33	0.28	0.15	0.04	2.96	0.25	1.998	-1.496
3C 236	-14.25	0.69	0.84	0.30	0.57	0.22	0.667	-3.368
3C 264	-14.35	1.45	0.66	0.22	0.33	0.27	0.313	-4.942
3C 270	-14.93	0.72	1.29	0.52	0.63	1.09	0.048	-5.145
3C 272.1	-13.57	1.28	0.86	0.23	0.19	0.10	0.478	-5.636
3C 274	-13.11	2.32	1.45	0.36	0.31	0.17	0.233	-5.240
3C 277.3	-14.43	0.79	0.60	0.29	1.29	0.19	1.119	-3.100
3C 285	-14.52	0.54	0.46	0.10	0.78	0.19	1.148	-3.332
3C 287.1	-14.62	0.68	0.58	0.48	1.71	0.27	1.043	-2.704
3C 288	-15.40	1.87	1.45	0.40	0.62	0.58	0.095	-3.961
3C 293	-14.49	0.88	1.32	0.26	0.42	0.19	0.518	-4.454
3C 296	-14.28	1.84	0.81	0.22	0.81	0.30	0.593	-4.803
3C 300	-14.58	0.48	0.56	0.15	1.71	0.25	1.300	-2.053
3C 303	-14.39	1.06	0.85	0.41	2.55	0.35	1.007	-2.523
3C 303.1	-14.24	1.03	0.86	0.24	2.07	0.26	1.125	
3C 305	-13.68	1.77	0.88	0.17	1.30	0.12	1.227	-3.191
3C 310	-14.50	1.74	1.58	0.30	0.54	0.23	0.399	-4.060
3C 314.1	-15.25	0.53	0.85	0.18	0.24	0.37	0.176	
3C 315	-14.32	0.72	0.88	0.25	0.53	0.20	0.690	-3.110
3C 317	-14.08	1.92	1.07	0.25	1.00	0.30	0.619	-4.233
3C 321	-14.87	0.50	0.33	0.06	2.58	0.30	1.603	-3.432
3C 323.1	-14.12	0.29	0.18	0.20	3.93	0.26	1.840	-2.108
3C 327	-13.70	0.73	0.54	0.14	3.20	0.27	1.493	
3C 332	-14.47	0.97	0.73	0.21	3.14	0.28	1.326	-2.467
3C 338	-14.11	1.63	0.74	0.18	0.21	0.18	0.288	-5.092
3C 349	-14.58	0.90	0.62	0.25	1.54	0.40	0.958	-2.327
3C 353	-13.90	1.09	0.99	0.30	0.53	0.20	0.587	-3.854
3C 371	-13.82	1.14	0.61	0.51	1.01	0.29	0.692	-3.327
3C 379.1	-14.89	1.54	0.58	0.21	2.80	0.31	1.198	-2.561

Notes: Column description: (1) Target name; (2)–(7) The flux of each narrow emission line in units of  $10^{-16}$  erg s $^{-1}$  cm $^{-2}$ .  
 ((4) Sum of blended [S II] $\lambda$   $\lambda$ 6716, 6731); (8) Excitation index value derived from Equation (1); (9)  $L_{\text{ion}}/L_{\text{Edd}}$  ratio.

**Table 2** — *Continued.*

Name (1)	H $\alpha$ (2)	[N II] $\lambda$ 6584 (3)	[S II] $\lambda$ $\lambda$ 6716, 6731 (4)	[O I] $\lambda$ 6300 (5)	[O III] $\lambda$ 5007 (6)	H $\beta$ (7)	EI (8)	$L_{\text{ion}}/L_{\text{Edd}}$ (9)
3C 382	-13.51	1.49	0.25	0.29	2.45	0.31	1.220	-2.798
3C 386	-13.63	0.57	0.19	0.10	1.08	1.08	0.655	-3.701
3C 388	-14.47	2.33	0.78	0.26	0.74	0.23	0.616	-3.957
3C 390.3	-13.29	0.47	0.20	0.27	3.24	0.32	1.537	-1.946
3C 401	-15.05	1.77	0.80	0.24	1.10	0.30	0.721	-3.064
3C 403	-13.71	0.84	0.49	0.13	3.54	0.25	1.575	-2.476
3C 403.1	-14.87	0.78	1.62	0.29	0.75	0.53	0.381	-3.943
3C 410	-14.40	1.04	0.67	0.18	1.46	0.12	1.472	
3C 424	-14.55	0.79	0.84	0.27	0.54	0.24	0.601	-2.818
3C 433	-14.01	1.09	0.76	0.22	1.88	0.19	1.242	-2.797
3C 442	-14.40	1.84	0.80	0.19	0.27	0.08	0.713	
3C 449	-14.09	1.38	0.51	0.13	0.30	0.10	0.823	-4.818
3C 452	-14.05	1.08	0.65	0.27	1.53	0.23	1.064	-2.723
3C 456	-13.72	0.78	0.46	0.15	2.15	0.32	1.250	
3C 458	-14.84	0.91	0.67	0.33	2.85	0.45	1.124	
3C 459	-13.97	1.77	0.68	0.12	0.73	0.16	0.939	-2.228
3C 460	-14.25	1.23	1.14	0.39	0.49	0.25	0.380	
3C 465	-14.17	2.77	0.79	0.26	0.46	0.17	0.514	-4.959
0025+006	-14.01	1.57	1.08	0.27	1.48	0.20	0.979	-1.873
0134+329	-13.43	0.30	0.12	0.08	1.65	0.28	1.633	-1.417
0221+276	-14.29	0.52	0.42	0.17	2.54	0.31	1.395	-2.357
0316+413	-12.47	1.23	1.15	0.91	2.25	0.20	1.010	-1.526
0345+337	-14.08	1.67	1.17	0.32	2.13	0.31	0.899	-2.368
0428+205	-14.40	1.36	0.96	0.68	0.52	0.09	0.799	-3.510
0605+480	-14.47	1.12	0.96	0.31	1.02	0.24	0.795	-3.549
0754+401	-13.97	0.91	0.59	0.13	1.73	0.19	1.337	-2.374
0810+077	-14.16	1.72	1.35	0.33	0.40	0.18	0.396	-3.817
0921+143	-14.38	2.31	1.91	0.62	0.31	0.33	-0.172	-4.061
0931+033	-14.57	1.28	1.07	0.26	0.60	0.17	0.709	-3.983
0941-080	-14.91	0.97	0.90	0.38	1.25	0.35	0.709	-2.600
1007+142	-14.87	2.65	1.88	0.57	0.54	0.36	0.031	-4.385
1037+302	-14.27	2.49	1.38	0.33	0.49	0.06	0.924	-3.733
1154+435	-14.20	0.47	0.40	0.08	3.14	0.30	1.629	-1.672
1203+645	-14.21	0.84	0.60	0.19	1.90	0.23	1.253	-1.921
1233+418	-14.43	0.71	1.02	0.37	1.10	0.31	0.742	-2.281
1250+568	-13.86	0.23	0.38	0.09	2.07	0.28	1.567	-1.585
1323+321	-14.71	1.22	0.87	1.13	4.03	0.36	1.027	-2.906
1345+125	-13.80	0.82	0.61	0.71	3.30	0.11	1.611	-1.263
1404+286	-14.06	1.03	0.60	0.26	2.47	0.23	1.290	-3.479
1407+363	-14.59	1.18	0.82	0.38	1.22	0.15	1.066	-2.799
1521+324	-14.80	2.10	0.92	0.26	1.96	0.14	1.230	-2.583
1558+536	-14.91	2.08	1.17	0.34	1.34	0.23	0.786	-3.497
1601+528	-14.75	1.63	1.80	0.44	0.72	0.15	0.658	-4.201
1610+407	-14.23	1.40	1.50	0.36	0.69	0.24	0.505	-3.067
1807+698	-13.90	1.08	0.52	0.63	0.83	0.20	0.774	-4.065
2352+495	-14.99	2.33	0.50	0.44	1.96	0.31	0.897	-3.334

We also compute the OLS fits for FR I sources, FR IIs and YRGs. The results are

$$\text{EI} = 0.213 \log \lambda_{\text{Edd}} + 1.34, \quad \text{for FR Is;} \quad (3)$$

$$\text{EI} = 0.522 \log \lambda_{\text{Edd}} + 2.42, \quad \text{for FR IIs;} \quad (4)$$

$$\text{EI} = 0.49 \log \lambda_{\text{Edd}} + 2.23, \quad \text{for YRGs.} \quad (5)$$

In addition, we check the correlation between EI and  $L_{\text{ion}}$ . The EI is found to correlate significantly with  $L_{\text{ion}}$ , with a Spearman correlation coefficient of  $\rho = 0.71$  and  $p = 3.99 \times 10^{-18}$  (see Fig. 2). According to the derived Spearman's correlation coefficient, we found that EI is better correlated with the Eddington ratio than the ionizing continuum.

#### 4 PHOTOIONIZATION MODEL CALCULATIONS

In order to understand the physics of the correlation between EI and Eddington ratio, we carry out photoionization model calculations using Cloudy version 10.01 (Ferland et al. 1998). For simplicity, we assume that gas clouds have uniform density with a plane-parallel geometry. The input parameters for the model calculations are: (a) the shape of the spectral energy distribution (SED) of the incident radiation field; (b) the chemical composition of the gas; (c) the constant hydrogen density ( $n_{\text{H}}$ ) throughout the cloud; (d) the luminosity of the incident radiation field; (e) The thickness of the cloud can be determined with the inner radius and the allowed maximum of column density which is assumed to be  $N_{\text{H}} = 10^{21} \text{ cm}^{-2}$ , since the column density of typical narrow-line region (NLR) clouds is not well known

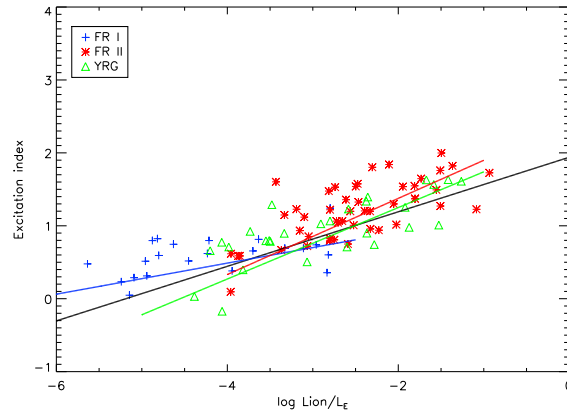


**Fig. 1** Relation between EI and Eddington ratio  $\lambda_{\text{Edd}}$  for radio galaxies. The black line is the best fit for all sources. The colored lines are for FR Is (blue), FR IIs (red) and YRGs (green).

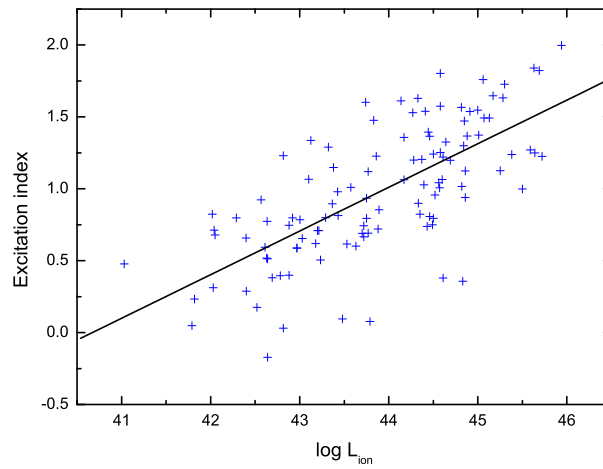


**Fig. 2** Relation between EI and ionizing continuum luminosity  $L_{\text{ion}}$  for radio galaxies. The black line is the best fit for all sources.

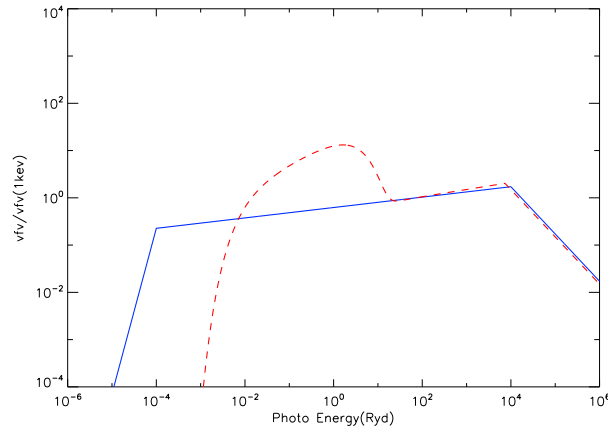


**Fig. 3** The SEDs adopted in our photoionization model calculations. The red dashed line represents an SED with a BBB, and the blue solid line represents an SED without a BBB. Both of the two SEDs are normalized to the flux at 1 keV ( $\approx 73$  Ryd).

but it is estimated to be smaller than the broad-line region column density of the order of  $10^{22}\text{cm}^{-2}$  (e.g. Blandford et al. 1990; Netzer 2015). For the ionizing continuum radiation, two types of SEDs are used: a typical SED with a strong big blue bump (BBB) and an SED without a BBB

(see Kawakatu et al. 2009). The first one mimics spectra of a standard accretion disk, while the second SED is typical for a radiatively inefficient accretion disk (see Fig. 3). Following Kawakatu et al. (2009), we adopt solar metallicity in all of our calculations.

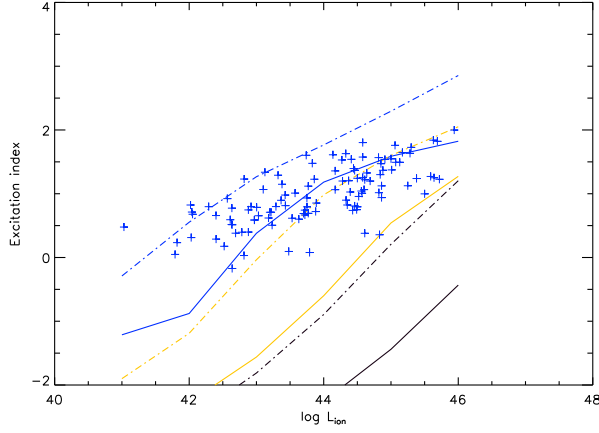


**Fig. 4** The results of the photoionizing model calculations for the ionizing SEDs both with and without a BBB, with the luminosities depending on sizes of the NLR. The solid lines are the results of SEDs without BBB models and the dashed lines are from models of SEDs with a BBB. The densities of clouds  $n_{\text{H}} = 10^2 \text{ cm}^{-3}$  (blue),  $n_{\text{H}} = 10^3 \text{ cm}^{-3}$  (yellow) and  $n_{\text{H}} = 10^4 \text{ cm}^{-3}$  (black) are adopted.

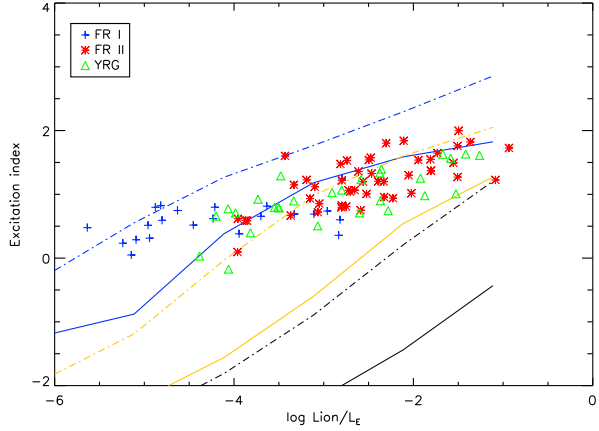


**Fig. 5** Same as Fig. 4 but for EI as a function of Eddington Ratio by assuming  $M_{\text{BH}} = 10^9 M_{\odot}$ .

We calculate the how EI varies with ionizing luminosity by assuming constant densities  $n_{\text{H}} = 10^2, 10^3$  or  $10^4 \text{ cm}^{-3}$  (e.g. Nagao et al. 2001) in the NLR. Liu et al. (2013) found a correlation between an extension of the relation between sizes of the NLRs and their [O III] luminosities

$$\begin{aligned} \log(R_{\text{int}}/\text{pc}) = & (0.250 \pm 0.018) \\ & \times \log(L_{[\text{O III}]} / 10^{42} \text{ erg s}^{-1}) \\ & + (3.746 \pm 0.028). \end{aligned} \quad (6)$$

(see Bennert et al. 2002; Liu et al. 2013). By assuming clouds in the NLR are distributed in a spherical geometry, the measured sizes of NLRs are taken as the inner radius of these NLRs.

Motivated by their works, we adopt this Luminosity - NLR size relation in our model. The resulting correlations between EI and ionizing luminosity are plotted in Figure 4 and they are sensitive to the assumed SEDs. In addition, in order to compare with the observed relationship between EI and Eddington Ratio (Fig. 1), we plot a new figure (Fig. 5) in which the modeled relations between EI

and Eddington Ratio  $L_{\text{ion}}/L_{\text{Edd}}$  are displayed, where we assume a constant black hole mass  $M_{\text{BH}} = 10^9 M_{\odot}$  by considering the black hole masses of the sources in Table 1.

Low-ionization nuclear emission regions (LINERs) are usually present in local galaxies with low Eddington ratio. By analyzing Hubble Space Telescope data of 23 LINERs and low luminosity Seyfert galaxies, Dai & Wang (2008) found that there was no significant difference between Seyfert galaxies and LINERs, with similar correlations between the NLR size and the narrow line luminosity. Moreover, the size of the  $\text{H}\alpha + [\text{N II}]$  emission line region was found to scale with  $\text{H}\alpha$  luminosity, which is the extension of the NLR size-luminosity relation defined for luminous Seyfert galaxies and quasars.

## 5 DISCUSSION

In this work, we use a sample of 111 radio galaxies with the redshift  $z < 0.3$  to investigate their nuclear properties. The black hole masses of the sources in this sample are estimated with the velocity dispersion/luminosity of the galaxies, or the widths of the broad-lines. There are differences

between FR I and FR II radio galaxies, such as the radio morphology and radio luminosity. Radio galaxies can also be classified into two subclasses according to their spectroscopic properties: HEGs and LEGs. The Eddington ratios of HEGs are systematically higher than those of LEGs. The EI is an indicator measuring the relative intensity of low and high excitation lines (Buttiglione et al. 2009). We find that the EI is significantly correlated with the Eddington ratio in our sample. The correlation is still present for the sub-samples (FR Is, FR IIs or YRGs), though the slopes are different (see Sect. 3).

In order to understand the physics of the correlation between EI and Eddington ratio which is found in Section 3, we perform photoionizing modeling with Cloudy. We find that such a correlation cannot be reproduced by the model calculations if a fixed NLR radius is adopted. Instead, if assuming the size of NLRs scales with ionizing luminosity as  $R_{\text{NLR}} \propto L_{\text{ion}}^{0.25}$  by Liu et al. (2013), the correlation can be reproduced. Two sets of SEDs, with or without BBB, have been adopted in our model calculations, respectively. The resulting correlations are found to be insensitive to the spectral shape (see Fig. 5).

As shown in Figure 5, the relation between EI and Eddington Ratio is insensitive to the assumed SED. This means that the difference between HEGs and LEGs may be not caused by the difference in accretion. As suggested by Liu et al. (2013), the size of an NLR varies with ionizing luminosity as  $R_{\text{NLR}} \propto L_{\text{ion}}^{0.25}$ , which implies the ionizing energy density  $U_{\text{ion}} \propto L_{\text{ion}}/R_{\text{NLR}}^{0.25} \propto L_{\text{ion}}^{0.5} \propto R_{\text{NLR}}^{0.25}$ . Therefore, the higher ionizing luminosity corresponds to larger ionizing energy density, yielding a stronger EI. This means that the difference between HEGs and LEGs is not caused by the different accretion modes, but rather is due to the intrinsic NLR sizes among these sources.

In this work, the NLR is assumed to be homogeneous with constant density. The inhomogeneity of the NLR which may consist of optically thin and thick gas (e.g., Kraemer et al. 1998; Nagao et al. 2000) will be taken into account in future works.

**Acknowledgements** This work is supported by the National Natural Science Foundation of China (Grant Nos. 11173043 and 11233006), the Strategic Priority Research Program “the Emergence of Cosmological Structures” of the CAS (Grant No. XDB09000000), and the CAS/SAFEA International Partnership Program for Creative Research Teams.

## References

- Baum, S. A., Zirbel, E. L., & O’Dea, C. P. 1995, *ApJ*, 451, 88  
 Bennert, N., Falcke, H., Schulz, H., Wilson, A. S., & Wills, B. J. 2002, *ApJ*, 574, L105  
 Bicknell, G. V. 1995, *ApJS*, 101, 29  
 Blandford, R. D., & Znajek, R. L. 1977, *MNRAS*, 179, 433  
 Blandford, R. D., Netzer, H., Woltjer, L., Courvoisier, T. J.-L., & Mayor, M., eds. 1990, *Active Galactic Nuclei*, 97  
 Blundell, K. M., & Rawlings, S. 2000, *AJ*, 119, 1111  
 Buttiglione, S., Capetti, A., Celotti, A., et al. 2009, *A&A*, 495, 1033  
 Buttiglione, S., Capetti, A., Celotti, A., et al. 2010, *A&A*, 509, A6  
 Cao, X., & Rawlings, S. 2004, *MNRAS*, 349, 1419  
 Dai, H.-F., & Wang, T.-G. 2008, *ChJAA (Chin. J. Astron. Astrophys.)*, 8, 245  
 Fanaroff, B. L., & Riley, J. M. 1974, *MNRAS*, 167, 31P  
 Ferland, G. J., Korista, K. T., Verner, D. A., et al. 1998, *PASP*, 110, 761  
 Ghisellini, G., & Celotti, A. 2001, *A&A*, 379, L1  
 Gopal-Krishna, & Wiita, P. J. 1988, *Nature*, 333, 49  
 Gopal-Krishna, & Wiita, P. J. 2000, *A&A*, 363, 507  
 Gültekin, K., Richstone, D. O., Gebhardt, K., et al. 2009, *ApJ*, 698, 198  
 Kaspi, S., Smith, P. S., Netzer, H., et al. 2000, *ApJ*, 533, 631  
 Kawakatu, N., Nagao, T., & Woo, J.-H. 2009, *ApJ*, 693, 1686  
 Kraemer, S. B., Crenshaw, D. M., Filippenko, A. V., & Peterson, B. M. 1998, *ApJ*, 499, 719  
 Laing, R. A., Jenkins, C. R., Wall, J. V., & Unger, S. W. 1994, in *Astronomical Society of the Pacific Conference Series*, 54, *The Physics of Active Galaxies*, eds. G. V. Bicknell, M. A. Dopita, & P. J. Quinn, 201  
 Ledlow, M. J., & Owen, F. N. 1996, *AJ*, 112, 9  
 Liu, G., Zakamska, N. L., Greene, J. E., Nesvadba, N. P. H., & Liu, X. 2013, *MNRAS*, 430, 2327  
 Marconi, A., & Hunt, L. K. 2003, *ApJ*, 589, L21  
 McGill, K. L., Woo, J.-H., Treu, T., & Malkan, M. A. 2008, *ApJ*, 673, 703  
 Nagao, T., Murayama, T., Taniguchi, Y., & Yoshida, M. 2000, *AJ*, 119, 620  
 Nagao, T., Murayama, T., & Taniguchi, Y. 2001, *ApJ*, 546, 744  
 Narayan, R., & Yi, I. 1994, *ApJ*, 428, L13  
 Netzer, H. 2015, *ARA&A*, 53, 365  
 O’Dea, C. P., Daly, R. A., Kharb, P., Freeman, K. A., & Baum, S. A. 2009, *A&A*, 494, 471  
 Reynolds, C. S., Fabian, A. C., Celotti, A., & Rees, M. J. 1996, *MNRAS*, 283, 873  
 Shakura, N. I., & Sunyaev, R. A. 1973, *A&A*, 24, 337  
 Shen, Y., Greene, J. E., Strauss, M. A., Richards, G. T., & Schneider, D. P. 2008, *ApJ*, 680, 169  
 Son, D., Woo, J.-H., Kim, S. C., et al. 2012, *ApJ*, 757, 140  
 Urry, C. M., & Padovani, P. 1995, *PASP*, 107, 803  
 Wold, M., Lacy, M., & Armus, L. 2007, *A&A*, 470, 531  
 Woo, J.-H., & Urry, C. M. 2002, *ApJ*, 579, 530  
 Wu, Q. 2009, *ApJ*, 701, L95  
 Xu, Y.-D., Cao, X., & Wu, Q. 2009, *ApJ*, 694, L107